2024 IEEE/RSJ International Conference on Intelligent Robots and Systems (IROS)
October 14-18, 2024. Abu Dhabi, UAE

Adaptive Passivation of Admittance Controllers by Bypassing Power to Null Space on Redundant Manipulators

Yeoil Yun, DongJun Oh, Eun Jeong Song, Hyouk Ryeol Choi, Hyungpil Moon, and Ja Choon Koo

Abstract— The significance of physical human-robot interaction (pHRI) with collaborative robots in the industry is growing steadily. Within this domain, an admittance controller is crucial for enabling robots to follow or assist human intentions. However, a persistent challenge with admittance controllers is ensuring their passivity. Various strategies have been developed to address this issue by adjusting the control signals derived from the admittance model. While these strategies achieve passivity, they often inadvertently impact collaborative performance, preventing the system from accurately aligning with the intended dynamics. Accordingly, this paper introduces an adaptive hierarchical control approach for redundant robots to handle this problem. This approach diverts non-passive power into the null space without diminishing the robot's responsiveness to human input. Implementing this null-space controller involves the dynamic adjustment of compliance control error, ensuring joint limit avoidance while facilitating integration with energy tanks for enhanced reliability. Moreover, the method enables the calculation of adaptive error gain in a closed form, simplifying its real-time application. Experimental validation with a 7-DOF manipulator showed a reduction of non-passive energy from 1.61 J to 0.12 J without compromising task performance.

I. Introduction

As a branch of modern robotics, physical human-robot interaction (pHRI) is growing in importance, driven by the need for robots that can interact safely and effectively with humans in various environments. The development of cooperative robots equipped with admittance controllers has enabled applications of pHRI, such as rehabilitation [1], [2], force augmentation [3], [4], [5], and teleoperation [6], [7], demonstrating the potential and versatility of its technologies. However, ensuring safety while interacting with humans is a prerequisite for pHRI. From this perspective, the robot's passivity plays a pivotal role in keeping human operators safe during operation [8]. Recent research's progress on passivity-based controllers highlights its importance for maintaining safe interactions between humans and robots, underscoring the need for reliable control mechanisms [9], [10].

Despite advancements in the admittance control scheme, stability challenges persist, particularly when the admittance parameters for inertia or damping are too low [11]. Additionally, the stability of the system can vary significantly depending on the force and velocity profiles taught by the human to the robot, and this human behavior is difficult to model in advance. As a result, a simple combination of an admittance controller and a PI controller alone cannot guarantee the negative definiteness of the total system energy when human interaction is involved. Solutions such as disturbance observer-based control [12], feed-forward strategies [13], and variable admittance [14], [15], [16] have been developed to address these issues. However, these approaches may lead to deviations from the initially intended robot motion, potentially making the generated path unpredictable and reducing the system's practicality in real-world applications. Ideally, robots should maintain predictable and consistent interactions with humans, closely following the pre-designed admittance model without sacrificing safety or performance.

The introduction of the energy tank method initially proposed in [17] offers an appropriate solution by defining a limit on the available system energy, allowing for controlled non-passivity to enhance performance. This approach increases the system's utility and flexibility in managing human interactions. For this reason, the energy tank method has been widely used in impedance or admittance control [18], [19], [20], [21]. Tank-based methods have also shown benefits in controlling redundant robots, facilitating the simultaneous execution of multiple task execution through the hierarchical controllers [9], [22], [23], [24]. By prioritizing effectively, redundant robots can be controlled with configurable strategies to take advantage of their null space. Also, due to the decoupling torque input introduced in [22], lower-priority tasks do not interfere with higher-priority tasks, allowing the controller of each task to be designed independently and increasing the robustness of the controlled system.

Therefore, this paper proposes a method of adaptively modifying the null-space dynamics using hierarchical controllers with energy tanks. This approach addresses critical issues such as the difficulty in maintaining passivity and the deviation from the initially intended dynamics due to performance degradation. The proposed controller ensures overall system passivity by applying an adaptive rule to the null-space dynamics, which dissipates excess energy generated in the system, excluding the null-space controller, when more energy is produced than the work done by the human. This mechanism is referred to as "non-passive power bypassing." Through

This work was supported by the National Research Foundation of Korea(NRF) grant funded by the Korea government(MSIT) (No. RS-2023-00209266).

The authors are with School of Mechanical Engineering, Sungkyunkwan University, Suwon, Korea. Corresponding author: Ja Choon Koo jckoo@skku.edu

this approach, the proposed controller ensures that human-robot interaction is predictable and consistent, closely following a pre-designed admittance model without compromising safety or performance. Additionally, the adaptation of the null-space dynamics not only dissipates excess energy from the system but is also designed to achieve effects similar to existing compliance control techniques for joint limit avoidance.

In the following sections, the architecture of the admittance controller based on end-effector motion and the null-space controller is described, and the passivity of the entire system is shown. Next, experiments using a 7-DOF manipulator (Franca Emika Panda) are presented for validation, demonstrating the feasibility of the proposed method to achieve the desired performance while maintaining system passivity.

II. Modeling and Analysis

A. Preliminaries

In order to deal with the robot's end effector motion task and null-space dynamics separately, the framework of a two-level hierarchical controller, first proposed in [22], is exploited. First, the dynamics of $n > 6$ joint redundant robots can be expressed as follows:

$$\boldsymbol{M}(\boldsymbol{q})\ddot{\boldsymbol{q}} + \boldsymbol{C}(\boldsymbol{q},\dot{\boldsymbol{q}})\dot{\boldsymbol{q}} + \boldsymbol{g}(\boldsymbol{q}) = \boldsymbol{\tau} + \boldsymbol{\tau}_h, \tag{1}$$

where $\boldsymbol{M}(\boldsymbol{q}) \in \mathbb{R}^{n\times n}$ is the symmetric positive definite inertia matrix, $\boldsymbol{C}(\boldsymbol{q},\dot{\boldsymbol{q}}) \in \mathbb{R}^{n\times n}$ is the Coriolis and centrifugal matrix, $\boldsymbol{g}(\boldsymbol{q}) \in \mathbb{R}^n$ is the gravitational torque, the joint motor torque is $\boldsymbol{\tau} \in \mathbb{R}^n$, and the torque exerted by the human on the robot joint is $\boldsymbol{\tau}_h \in \mathbb{R}^n$. To define the end effector twist for 6-DOF out of the total n-DOF of the robot and apply the null-space compliance control rule for the remaining $(n-6)$-DOF, The Jacobian $\boldsymbol{J}(\boldsymbol{q}) \in \mathbb{R}^{6\times n}$ that maps the 6-DOF end effector Cartesian motion task $\boldsymbol{x} = \boldsymbol{f}(\boldsymbol{q})$ to joint space is expressed as

$$\dot{\boldsymbol{x}} = \boldsymbol{J}(\boldsymbol{q})\dot{\boldsymbol{q}}, \quad \boldsymbol{J}(\boldsymbol{q}) = \frac{\partial \boldsymbol{f}}{\partial \boldsymbol{q}}. \tag{2}$$

Next, the extended Jacobian $\boldsymbol{J}_e(\boldsymbol{q}) \in \mathbb{R}^{n\times n}$ of the full-rank square matrix is defined for the extended space velocity vector

$$\dot{\boldsymbol{x}}_e = \begin{bmatrix} \dot{\boldsymbol{x}} \\ \dot{\boldsymbol{x}}_n \end{bmatrix} = \begin{bmatrix} \boldsymbol{J}(\boldsymbol{q}) \\ \boldsymbol{N}(\boldsymbol{q}) \end{bmatrix} \dot{\boldsymbol{q}} = \boldsymbol{J}_e(\boldsymbol{q})\dot{\boldsymbol{q}}, \tag{3}$$

where $\dot{\boldsymbol{x}}_n \in \mathbb{R}^{n-6}$ is the null-space velocity vector decoupled from $\dot{\boldsymbol{x}}$, and $\boldsymbol{N}(\boldsymbol{q}) = (\boldsymbol{Z}\boldsymbol{M}\boldsymbol{Z}^T)^{-1}\boldsymbol{Z}\boldsymbol{M}$ is the null-space Jacobian matrix that makes $\boldsymbol{J}_e$ non-singular. The $\boldsymbol{Z}$ used here is the base matrix that spans the null space of $\boldsymbol{J}^T$. The expression transformed from (1) to extended space dynamics using $\boldsymbol{J}_e$, with $\dot{\boldsymbol{x}}_e$ as the new coordinate, is

$$\boldsymbol{\Lambda}_e\ddot{\boldsymbol{x}}_e + \boldsymbol{\mu}_e\dot{\boldsymbol{x}}_e = \boldsymbol{J}_e^{-T}\big(-\boldsymbol{g}(\boldsymbol{q}) + \boldsymbol{\tau} + \boldsymbol{\tau}_h\big), \tag{4}$$

where extended space inertia $\boldsymbol{\Lambda}_e = \boldsymbol{J}_e^{-T}\boldsymbol{M}\boldsymbol{J}_e^{-1}$, and the extended space Coriolis and centrifugal matrix can be expressed by the following formulas and submatrix:

$$\boldsymbol{\mu}_e = \boldsymbol{\Lambda}_e\left(\boldsymbol{J}_e\boldsymbol{M}^{-1}\boldsymbol{C} - \dot{\boldsymbol{J}}_e\right)\boldsymbol{J}_e^{-1} = \begin{bmatrix} \boldsymbol{\mu}_x & \boldsymbol{\mu}_{xn} \\ \boldsymbol{\mu}_{nx} & \boldsymbol{\mu}_n \end{bmatrix}. \tag{5}$$

In (5), $\boldsymbol{\mu}_x \in \mathbb{R}^{6\times 6}$ and $\boldsymbol{\mu}_n \in \mathbb{R}^{n-6\times n-6}$ are the block diagonal parts of $\boldsymbol{\mu}_e$. The off-diagonal parts of $\boldsymbol{\mu}_{xn}$ and $\boldsymbol{\mu}_{nx}$ cause velocity coupling of the two tasks, and the torque to decouple this effect is

$$\boldsymbol{\tau}_\mu = \boldsymbol{J}_e^T\begin{bmatrix} 0 & \boldsymbol{\mu}_{xn} \\ \boldsymbol{\mu}_{nx} & 0 \end{bmatrix}\boldsymbol{J}_e\dot{\boldsymbol{q}} \tag{6}$$

where $\boldsymbol{\mu}_{xn}^T = -\boldsymbol{\mu}_{nx}$. This property makes the input power $\dot{\boldsymbol{q}}^T\boldsymbol{\tau}_\mu = 0$, so it is possible to decouple the effects of the two tasks passively by adding $\boldsymbol{\tau}_\mu$ to the torque input. As a result, summing the torques computed from the two tasks, the gravity compensating and the velocity decoupling torque, the input commanded torque becomes

$$\boldsymbol{\tau} = \boldsymbol{g}(\boldsymbol{q}) + \boldsymbol{J}^T\boldsymbol{F}'_a + \boldsymbol{N}^T\boldsymbol{Z}\boldsymbol{F}'_n + \boldsymbol{\tau}_\mu, \tag{7}$$

where $\boldsymbol{F}'_a \in \mathbb{R}^6$ is the wrench computed from the admittance controller and velocity PI controller, and $\boldsymbol{F}'_n \in \mathbb{R}^n$ is the joint space force. The following sections will describe how each of these control inputs is computed.

B. Formulations and Passivity Analysis

Here, the methodology of bypassing the non-passive power generated by the 6-DOF end effector admittance controller, a higher priority task, to the null-space task will be described while simultaneously showing the overall system passivity using the energy tank and adaptive gain tuner. First, the virtual dynamics of the robot is represented by the following admittance model:

$$\bar{\boldsymbol{\Lambda}}\ddot{\boldsymbol{x}}_d + \bar{\boldsymbol{\mu}}\dot{\boldsymbol{x}}_d = \boldsymbol{F}'_e, \tag{8}$$

where $\boldsymbol{x}_d \in \mathbb{R}^6$ is the desired Cartesian motion profile of the end effector, $\bar{\boldsymbol{\Lambda}} \in \mathbb{R}^{6\times 6}$ is the virtual mass of the robot, $\bar{\boldsymbol{\mu}} \in \mathbb{R}^{6\times 6}$ is the virtual damping coefficient. The force input $\boldsymbol{F}'_e = \sigma\boldsymbol{F}_e$ is the adjusted external force $\boldsymbol{F}_e$ obtained through sensors (or estimators) using the energy tank level dependent coefficient σ.

The velocity PI controller was used as the inner controller to follow the desired trajectory $\dot{\boldsymbol{x}}_d$ obtained in (8), so the desired force in the task space can be expressed as follows:

$$\boldsymbol{F}_a = \boldsymbol{K}_{a,p}\dot{\tilde{\boldsymbol{x}}}' + \boldsymbol{K}_{a,i}\tilde{\boldsymbol{x}}' \tag{9}$$

where $\tilde{\boldsymbol{x}} = \boldsymbol{x}_d - \boldsymbol{x}$, and $(\cdot)'$ means that another regulating coefficient controls the state to ensure passivity, which will be explained later. The null-space task input force that makes joint angles restore the desired pose is

$$\boldsymbol{F}_n = \boldsymbol{K}_{n,p}\tilde{\boldsymbol{q}}' + \boldsymbol{K}_{n,d}\dot{\tilde{\boldsymbol{q}}}'. \tag{10}$$

In (9) and (10), $\boldsymbol{K}_{a,p}, \boldsymbol{K}_{a,i} \in \mathbb{R}^{6\times 6}$ and $\boldsymbol{K}_{n,p}, \boldsymbol{K}_{n,d} \in \mathbb{R}^{n\times n}$ are all positive definite matrices. The error vector between the joint angle and the desired joint angle is

$\bar{\boldsymbol{q}} = \boldsymbol{q}_d - \boldsymbol{q}$, and the joint angle error multiplied by the adaptive gain β, which is the modulated joint angle error, is $\tilde{\boldsymbol{q}} = \beta\bar{\boldsymbol{q}}$. Thus, β is used to control the magnitude of the error adaptively, ensuring that the system does not become non-passive. The $\boldsymbol{F}_a$ and $\boldsymbol{F}_n$ calculated by the above formulas are regulated based on the energy tank in such a way that they are converted to $\boldsymbol{F}'_a = \sigma\boldsymbol{F}_a$ and $\boldsymbol{F}'_n = \sigma\boldsymbol{F}_n$, and then passed to (7). Next, the total energy of the system, which can be derived from the equations set up so far, is

$$\begin{aligned} S =& \frac{1}{2}\dot{\boldsymbol{x}}_e^T\boldsymbol{\Lambda}_e\dot{\boldsymbol{x}}_e + \frac{1}{2}\dot{\bar{\boldsymbol{x}}}_d^T\bar{\boldsymbol{\Lambda}}\dot{\bar{\boldsymbol{x}}}_d \\ &+ \frac{1}{2}\tilde{\boldsymbol{x}}'^T\boldsymbol{K}_{a,i}\tilde{\boldsymbol{x}}' + \frac{1}{2}\tilde{\boldsymbol{q}}'^T\boldsymbol{K}_{n,p}\tilde{\boldsymbol{q}}' + E_t, \end{aligned} \tag{11}$$

and due to the terms expressed in quadratic form, it is obvious that if E_t is positive definite, then S becomes positive definite. Now, using (8), (9) and (10), and with the property $\dot{\boldsymbol{M}}(\boldsymbol{q}) = \boldsymbol{C}(\boldsymbol{q},\dot{\boldsymbol{q}}) + \boldsymbol{C}(\boldsymbol{q},\dot{\boldsymbol{q}})^T$, the time derivative of S is defined as

$$\begin{aligned} \dot{S} =& \dot{\boldsymbol{q}}^T\boldsymbol{\tau}_h \overbrace{+ \dot{\boldsymbol{x}}^T\boldsymbol{F}'_a + \dot{\boldsymbol{x}}_n^T\boldsymbol{Y}\boldsymbol{F}'_n + \dot{\boldsymbol{x}}_d^T\boldsymbol{F}'_e}^{\dot{E}_r} \\ &\overbrace{+ \dot{\tilde{\boldsymbol{x}}}'^T\boldsymbol{F}_a}^{\dot{E}_b} + \dot{\tilde{\boldsymbol{q}}}'^T\boldsymbol{K}_{n,p}\tilde{\boldsymbol{q}}' \\ &\overbrace{- \dot{\boldsymbol{x}}_d^T\bar{\boldsymbol{\mu}}\dot{\boldsymbol{x}}_d - \dot{\tilde{\boldsymbol{x}}}'^T\boldsymbol{K}_{a,p}\dot{\tilde{\boldsymbol{x}}}'}^{\dot{E}_c} + \dot{E}_t, \end{aligned} \tag{12}$$

where E_r is the energy regulated by the tank, E_b is the energy to be adaptively compensated, which are the terms that are bypassed to null space, and E_c are the negative definite terms that serve to keep the energy tank and null-space gain from being depleted. Next, the energy tank is charged or discharged by the rule of

$$\dot{E}_t = \begin{cases} 0 & \text{if } E_t \geq E_{t,max} \\ -\dot{E}_r - \alpha\dot{E}_c & \text{otherwise,} \end{cases} \tag{13}$$

which implies that the energy of the system is continuously monitored when the energy tank level is within the specified range $(0, E_{t,max})$, and then the incoming power is dissipated when the level reaches the maximum $E_{t,max}$. When the tank level is within the bounds, each energy variable $E_{(\cdot)}$ can be expressed in terms of effort $x_{(\cdot)}$ and flow $\dot{x}_{(\cdot)}$, which can be represented as $E_{(\cdot)} = \frac{1}{2}{x_{(\cdot)}}^2$. Consequently, the relationship can be simplified as follows:

$$\begin{bmatrix} \dot{x}_r \\ \dot{x}_c \\ x_t \end{bmatrix} = \frac{1}{\dot{x}_t}\begin{bmatrix} 0 & 0 & \dot{x}_r \\ 0 & 0 & \dot{x}_c \\ -\dot{x}_r & -\dot{x}_c & 0 \end{bmatrix}\begin{bmatrix} x_r \\ \alpha x_c \\ \dot{x}_t \end{bmatrix} \tag{14}$$

Therefore, in (14), the power conversion relationship of the multiport junction is represented by a skew-symmetric matrix, which implies that the energy exchanged during the charging and discharging process of the energy tank is conserved.

Here, α is a variable greater than 0 and less than 1 that regulates the ratio of energy tank charge and β compensation, i.e,

$$\alpha = \frac{\beta}{\beta + E_t/E_{t,max}}, \tag{15}$$

and can be regarded as the principle of charging the more discharged side at a larger ratio. Then, the regulating coefficient

$$\sigma = \begin{cases} 0 & \text{if } E_t \leq 0 \\ 1 & \text{otherwise} \end{cases} \tag{16}$$

is set to limit the power of $\dot{E}_r$ so that the tank level can no longer decrease when the energy tank is depleted. It ensures that E_t is always within the bound between 0 and $E_{t,max}$, leading to S always being positive definite.

In contrast to $\dot{E}_r$, which can easily control the tank level through input effort regulation, the end effector velocity error and null-space angle error dynamics are determined by the flow input, as shown in (9) and (10). Therefore, instead of including these two powers in the energy tank's charge and discharge expressions, the power from these two dynamics is mutually canceled out by monitoring E_b and adaptively varying $\dot{\tilde{\boldsymbol{q}}}'^T\boldsymbol{K}_{n,p}\tilde{\boldsymbol{q}}'$. So now it is necessary to determine the rule of β to create the appropriate $\dot{\tilde{\boldsymbol{q}}}'^T\boldsymbol{K}_{n,p}\tilde{\boldsymbol{q}}'$. For the excluded part of the previous proof of passivity with energy tanks, for all $t \geq 0$, the inequality

$$\dot{E}_b + (1-\alpha)\dot{E}_c + \dot{\tilde{\boldsymbol{q}}}'^T\boldsymbol{K}_{n,p}\tilde{\boldsymbol{q}}' \leq 0 \tag{17}$$

must be shown to be satisfied to prove complete passivity. Integrating the above expression gives for all $t \geq 0$

$$2\int_0^t -\dot{E}_b - (1-\alpha)\dot{E}_c\,dt \geq \tilde{\boldsymbol{q}}'^T\boldsymbol{K}_{n,p}\tilde{\boldsymbol{q}}' \tag{18}$$

and since $\tilde{\boldsymbol{q}} = \beta\bar{\boldsymbol{q}}$, If

$$\beta = \sqrt{\frac{w_2}{w_1}}, \tag{19}$$

where

$$w_1 = \frac{1}{2}\bar{\boldsymbol{q}}^T\boldsymbol{K}_{n,p}\bar{\boldsymbol{q}} \tag{20a}$$

$$w_2 = \int_0^t -\dot{E}_b - (1-\alpha)\dot{E}_c\,dt + w_1|_{t=0}, \tag{20b}$$

then (18) always satisfies the equation. The last term $w_1|_{t=0}$ on the right-hand side of (20b) is the supplementary value for initializing w_2 to set $\beta = 1$ at $t = 0$ by simply computing and adding w_1 at $t = 0$. Since the null-space controller does not affect the higher priority task, it can be assumed that the robot pose does not reach the desired position perfectly and is always $\bar{\boldsymbol{q}} \neq 0$. Under this condition, it is obvious that it is always $w_1 > 0$, but if $w_2 \leq 0$, there may be a problem that (19) cannot

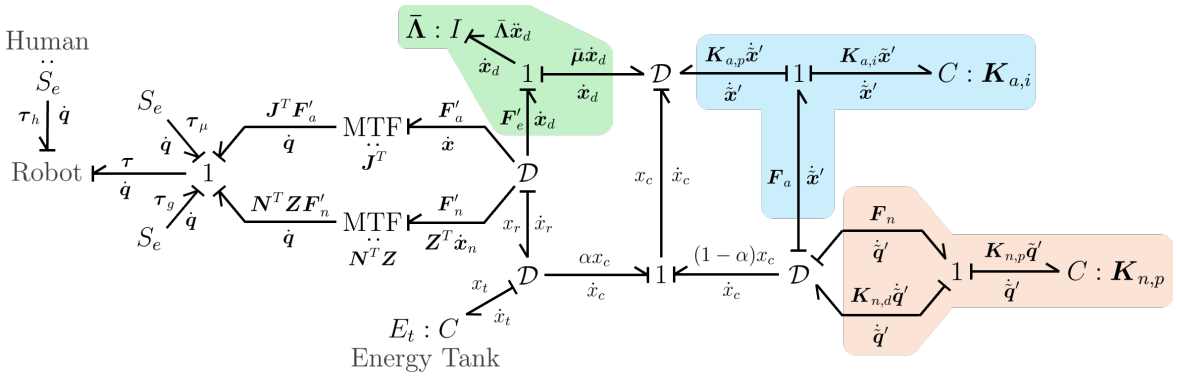

Fig. 1. Bond graph of the entire system. The 1-junction highlighted in the background corresponds to, from left to right, admittance, velocity PI controller, and null-space joint angle PD controller dynamics. The $\mathcal{D}$ is a Dirac structure, with the property that the input and output energy is conservative for the connected ports.

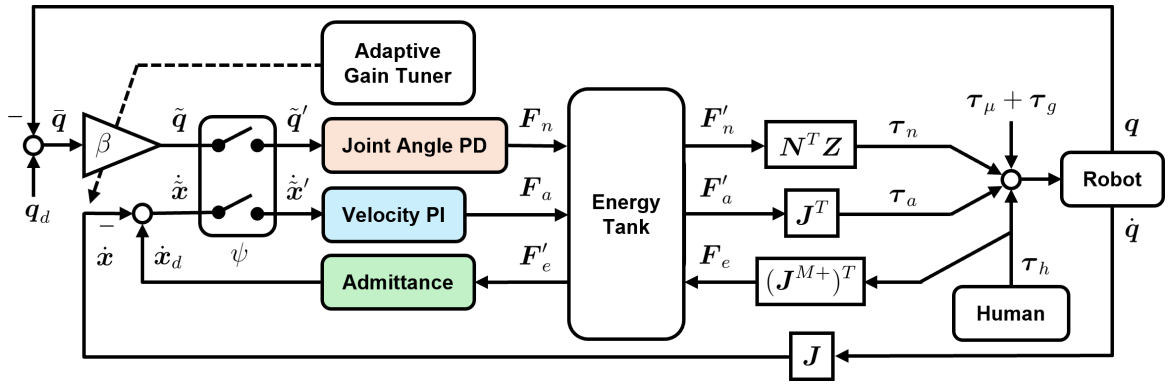

Fig. 2. A block diagram of the proposed controller. $\boldsymbol{J}^{M+} = \boldsymbol{M}^{-1}\boldsymbol{J}^T(\boldsymbol{J}\boldsymbol{M}^{-1}\boldsymbol{J}^T)$ is the inertia weighted pseudoinverse of $\boldsymbol{J}$. Any of the force $\boldsymbol{F}$ entering through the energy tank becomes $\boldsymbol{F}'$ after being regulated by multiplying σ.

be defined. So, using a similar approach to tank-level regulation, another regulating coefficient

$$\psi = \begin{cases} 0 & \text{if } \beta \leq 0 \\ 1 & \text{otherwise} \end{cases} \tag{21}$$

could be used for (9) and (10) to define a regulated flow $(\cdot)' = \psi(\cdot)$. Now, by applying (21) to $\dot{\boldsymbol{q}}$ and $\dot{\boldsymbol{x}}$, it can be guaranteed that $w_2 \geq 0$ for all cases. Finally, applying all of the above rules and grouping the terms in (12) that cancel each other out, it becomes

$$\begin{aligned} \dot{S} =& \dot{\boldsymbol{q}}^T\boldsymbol{\tau}_h \overbrace{+ \dot{E}_r + \alpha\dot{E}_c + \dot{E}_t}^{\text{Negative Definite}} \\ & \overbrace{+ \dot{E}_b + (1-\alpha)\dot{E}_c + \dot{\tilde{\boldsymbol{q}}}'^T\boldsymbol{K}_{n,p}\tilde{\boldsymbol{q}}'}^{\text{Negative Definite}} \end{aligned} \tag{22}$$

which proves the passivity of S for the input-output pair $(\boldsymbol{\tau}_h, \dot{\boldsymbol{q}})$. The bond graph representation of the entire system is shown in Fig. 1, and it can be seen that causality is satisfied throughout the system. A schematic of the controller using a block diagram for clarity can also be found in Fig. 2.

III. Experiments

In order to verify the performance of the proposed controller, the same task was performed with an adaptive controller and a controller with constant gain, i.e., a conventional null-space compliance controller, and the results were compared. The constant gain controller to be compared is the same as the one with $\beta = 1$ for all times in (10). However, an energy tank was also used for this controller for a more straightforward comparison. First, in addition to the representation in (12), the $\dot{S}$ shown earlier can also be described as follows:

$$\begin{aligned} \dot{S} =& \dot{\boldsymbol{q}}^T\boldsymbol{\tau}_h \\ & \overbrace{+ \dot{\boldsymbol{x}}^T\boldsymbol{F}'_a + \dot{\boldsymbol{x}}_n^T\boldsymbol{Y}\boldsymbol{F}'_n + \dot{\boldsymbol{x}}_d^T\boldsymbol{F}'_e + \dot{\tilde{\boldsymbol{x}}}'^T\boldsymbol{F}_a + \dot{\tilde{\boldsymbol{q}}}'^T\boldsymbol{F}_n}^{\dot{E}_r} \\ & \overbrace{- \dot{\boldsymbol{x}}_d^T\bar{\boldsymbol{\mu}}\dot{\boldsymbol{x}}_d - \dot{\tilde{\boldsymbol{x}}}'^T\boldsymbol{K}_{a,p}\dot{\tilde{\boldsymbol{x}}}' - \dot{\tilde{\boldsymbol{q}}}'^T\boldsymbol{K}_{n,d}\dot{\tilde{\boldsymbol{q}}}'}^{\dot{E}_c} + \dot{E}_t. \end{aligned} \tag{23}$$

The charging and discharging rule for the constant gain controller's energy tank can also be set similarly to (13), which is given by

$$\dot{E}_t = \begin{cases} 0 & \text{if } E_t \geq E_{t,max} \\ -\dot{E}_r - \dot{E}_c & \text{otherwise.} \end{cases} \tag{24}$$

(24) means that the negative definite powers are not modulated using α and are all used to fill the energy tank. Therefore, monitoring the tank level makes it possible

to determine if the entire system is exhibiting passive or non-passive behavior. For the proposed controller, the power canceled by the adaptive gain due to (22) will always be zero for $\sigma = \psi = 1$, so comparing the energy tank levels of the two controllers can be used to determine how passive the controller and robot are behaving.

A. Experimental Setup

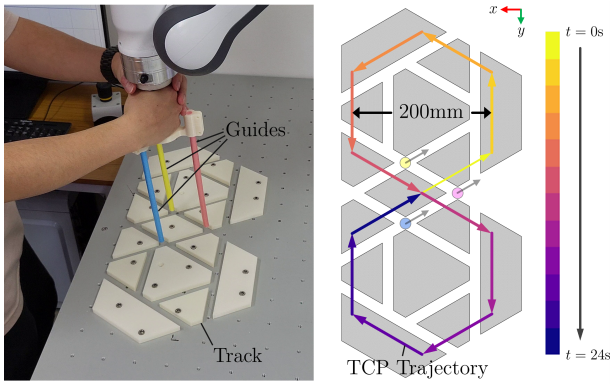

Fig. 3. An experimental setup. In order to keep the robot's posture as consistent as possible throughout the interaction, three poles and a track corresponding to each pole were used as visual aids to guide the robot to perform the same task. The end effector was moved along a path of two connected hexagons, and a force was applied to the robot so that each side of the hexagon took two seconds to move.

The experiments were conducted using a Franka Emika Panda 7-DOF manipulator, and the controller was implemented using ROS to run at 1 kHz. To validate the controller's performance in the context of compliant motion with human-applied forces, a human force was applied to the robot by holding the manipulator's end effector and forcing it to move along a specific trajectory. The starting point and path of the tool center point (TCP) are shown in Fig. 3. In order to make the task as identical as possible between the two experiments, the experiment was conducted by teaching the same path as much as possible based on the three pillar-shaped guides. The path was set to the task of drawing two hexagons on the x-y plane, and a metronome aided the human's teaching speed to ensure that each side of the hexagon took 2 seconds. This experiment measured the human's force using the momentum observer [25]. This results in the transfer function of the real human torque and the estimated torque having a relationship of

$$\frac{\hat{\boldsymbol{\tau}}_h(s)}{\boldsymbol{\tau}_h(s)} = \frac{k_{MOB}}{s + k_{MOB}}, \tag{25}$$

but this does not disturb the proof of passivity shown above because the phase lag of $(\boldsymbol{\tau}_h, \hat{\boldsymbol{\tau}}_h)$ is always between $\pm 90°$, so the entire system remain passive [26]. The parameters of the controller used in both experiments were set to be the same except for the adaptive gain, which is shown in Table I, where $\boldsymbol{q}_d$ is set to the midpoint of the upper and lower limits of each joint angle.

TABLE I
Controller Parameters

parameters	value	unit
Λ	1	kg
$\bar{\mu}$	10	Ns/m
k_{MOB}	10	-
$\boldsymbol{K}_{a,p}$	$10 \cdot \boldsymbol{I}_{6\times6}$	-
$\boldsymbol{K}_{a,i}$	$10 \cdot \boldsymbol{I}_{6\times6}$	-
$\boldsymbol{K}_{n,p}$	$2 \cdot \boldsymbol{I}_{7\times7}$	-
$\boldsymbol{K}_{n,d}$	$2 \cdot \boldsymbol{I}_{7\times7}$	-
$E_{t,i}$	10	J
$E_{t,max}$	20	J
$\boldsymbol{q}_d$	$[0, 0, 0, -0.5\pi, 0, 0.8\pi, 0]^T$	rad

B. Results

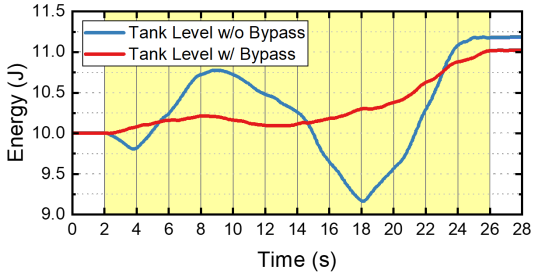

Fig. 4. Changes in energy tank levels in two experiments. The interval marked by the colored background is where the interaction with the person took place.

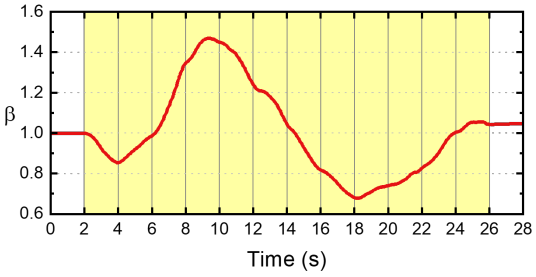

Fig. 5. The change in adaptive error gain β between experiments on a controller with null-space bypass. The interval marked by the colored background is where the interaction with the person took place.

In Fig. 4, both experiments show that the initial energy tank level starts at $E_{t,i} = 10$ J, ending at 11.18 J for the controller without bypass and 11.02 J with bypass. The maximum peak-to-peak decrease during the 2 s to 26 s interval of human interaction was about 1.61 J from 8.97 s to 18.12 s for the controller without bypass, while the maximum decrease in energy tank level was about 0.12 J from 8.21 s to 13.07 s for the controller with adaptively bypassing power to null space. The β calculated by (19) during the same experiment is shown in Fig. 5. Its value started at 1.000 and ended at 1.043 after the task ended, increasing by a maximum of 1.469 in 9.36 seconds and decreasing by a minimum of 0.678 in 18.22 seconds. The sum of the admittance storage E_a and

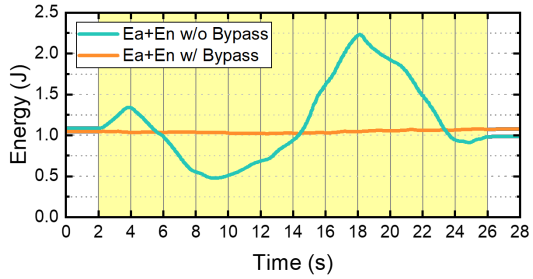

Fig. 6. Comparison of the sum of the storage energy in the admittance controller and the null-space controller, with and without adaptive gain.

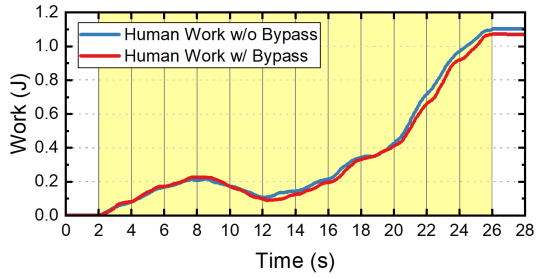

Fig. 7. The work done by the human to the robot in each of the two experiments. The interval marked by the colored background is where the interaction with the person took place.

null-space controller storage E_n during the interaction with the human is shown in Fig. 6. In this result, the maximum peak-to-peak difference was approximately 0.059 J with the bypass and approximately 1.757 J without the bypass.

Next, a graph showing the work done by the human to the robot $\int_0^t \dot{\boldsymbol{q}}^T \boldsymbol{\tau}_h \, dt$ for the same experiment is shown in Fig. 7. Without bypass, the human did 1.10 J of work by the end of the experiment, while with bypass, the human did 1.07 J of work. When comparing the two tasks, the root mean square error (RMSE) during the human interaction is 0.03 J and the maximum absolute error is 0.08 J. Finally, in Fig. 8, graphs of $||\boldsymbol{q}_d - \boldsymbol{q}||_2$ for both experiments and $\beta||\boldsymbol{q}_d - \boldsymbol{q}||_2$ for the experiment

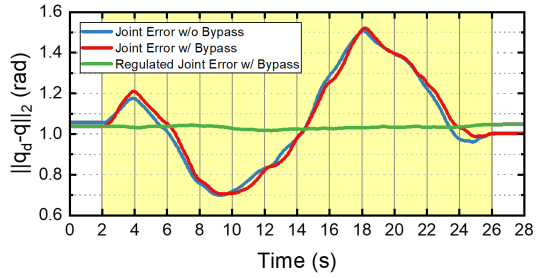

Fig. 8. The L_2 norm computed from the error vector between the joint angle and the desired angle across all seven joints, which is the $||\boldsymbol{q}_d - \boldsymbol{q}||_2 = \sqrt{(\boldsymbol{q}_d - \boldsymbol{q})^T(\boldsymbol{q}_d - \boldsymbol{q})}$ for the two experiments. And $\beta||\boldsymbol{q}_d - \boldsymbol{q}||_2$ of the experiment with bypass is also represented. The interval marked by the colored background is where the interaction with the person took place.

with bypass can be seen. The L_2 norm RMSE for both experiments is 0.026 rad, and the maximum absolute error is 0.057 rad. The $\beta||\boldsymbol{q}_d - \boldsymbol{q}||_2$ shows that the magnitude of the regulated error norm ranges from a minimum of 1.017 rad to a maximum of 1.050 rad, with an average of 1.034 rad.

IV. Discussion

From Fig. 7, it is observed that the work exerted by the human on the robot in both experiments is nearly identical, indicating that the energy generated by the robot controller to support the human effort is similar in both cases. This result suggests a minimal difference in admittance controller performance, regardless of the bypass implementation. However, as shown in Fig. 4, a notable reduction in E_t occurs when non-passive power is not bypassed, causing the system to behave non-passively. In contrast, with the bypass implemented, E_t exhibits a comparatively smaller reduction, indicating more passive behavior from both the robot and the controller. The effectiveness of the bypass in achieving system passivation is more clearly demonstrated in Fig. 6, where the fluctuations in the storage energy of E_a and E_n are reduced. This reduction was achieved by regulating the total system energy through the null-space gain, which can be interpreted as using an additional energy reservoir to buffer the overall system energy fluctuations in addition to the energy tank. These findings demonstrate that the proposed method effectively transfers non-passive energy to the null-space compliance controller. Moreover, maintaining constant admittance inertial parameters and damping coefficients preserved the robot's intended dynamics.

Additionally, Fig. 8 illustrates that the angular error norm remains consistent whether a bypass is used. This result is partly due to the projection of $\boldsymbol{F}'_n$ into a lower dimension with $\boldsymbol{N}^T\boldsymbol{Z}$, significantly reducing its influence. However, another critical factor in achieving this consistency is the application of (20a), which normalizes the whole joint angular error vector. This normalization maintains the error correction weights for each joint, ensuring the controller's effectiveness in implementing joint limit avoidance strategies. Consequently, $\beta||\boldsymbol{q}_d - \boldsymbol{q}||_2$ observed in Fig. 8 exhibits minimal fluctuations, staying close to a value of 1. The stability of this regulated error norm is attributed to the relatively small changes in the value of (20b) throughout experiments in this paper. Despite these phenomena, the angle-based PD controller effectively prevented the robot from reaching its angular joint limits. This outcome indicates that the controller can fulfill multiple functions within redundant robotic systems, obviating the need for additional null-space control rules. Moreover, it highlights the controller's potential for straightforward integration into universal hierarchical controller frameworks.

V. Conclusion

This paper proposes a method to mitigate the non-passive behavior of the admittance controller by adjusting the compliance controller's error state within the null space of a redundant robot. This approach can maintain interactive performance by incorporating an energy tank method while ensuring passivity. While the null-space dynamics change arbitrarily, The admittance parameter was kept constant during the controller's design, facilitating seamless human-robot interaction according to the intended dynamics. Moreover, through a hierarchical control framework, it was shown that two tasks with different priorities could operate simultaneously without interference. The adaptive gain was calculated using closed-form expressions only involving square roots, numerical integration, and algebraic operations, enabling real-time control. This capability was verified through experimental validation. These results suggest a path forward for research to improve robotic controllers' adaptability and operational efficiency in pHRI environments.

Acknowledgement

This work was supported by the National Research Foundation of Korea(NRF) grant funded by the Korea government(MSIT) (No. RS-2023-00209266).

References

[1] G. Li, L. Cheng, Z. Gao, X. Xia, and J. Jiang, "Development of an untethered adaptive thumb exoskeleton for delicate rehabilitation assistance," IEEE Transactions on Robotics, vol. 38, no. 6, pp. 3514–3529, 2022.

[2] Q. Wu, X. Wang, B. Chen, and H. Wu, "Development of a minimal-intervention-based admittance control strategy for upper extremity rehabilitation exoskeleton," IEEE Transactions on Systems, Man, and Cybernetics: Systems, vol. 48, no. 6, pp. 1005–1016, 2017.

[3] M. J. Kim, W. Lee, J. Y. Choi, G. Chung, K.-L. Han, I. S. Choi, C. Ott, and W. K. Chung, "A passivity-based nonlinear admittance control with application to powered upper-limb control under unknown environmental interactions," IEEE/ASME Transactions on Mechatronics, vol. 24, no. 4, pp. 1473–1484, 2019.

[4] W. Zou, X. Chen, S. Li, P. Duan, N. Yu, and L. Shi, "Robust admittance control for human arm strength augmentation with guaranteed passivity: A complementary design," IEEE/ASME Transactions on Mechatronics, vol. 27, no. 6, pp. 5936–5947, 2022.

[5] K. Haninger, M. Radke, A. Vick, and J. Krüger, "Towards high-payload admittance control for manual guidance with environmental contact," IEEE Robotics and Automation Letters, vol. 7, no. 2, pp. 4275–4282, 2022.

[6] D. Lee, D. Ko, W. K. Chung, and K. Kim, "Quadratic programming-based task scaling for safe and passive robot arm teleoperation," IEEE/ASME Transactions on Mechatronics, vol. 27, no. 4, pp. 1937–1945, 2022.

[7] Z. Ma, Z. Liu, P. Huang, and Z. Kuang, "Adaptive fractional-order sliding mode control for admittance-based telerobotic system with optimized order and force estimation," IEEE Transactions on Industrial Electronics, vol. 69, no. 5, pp. 5165–5174, 2021.

[8] A. Q. Keemink, H. van der Kooij, and A. H. Stienen, "Admittance control for physical human–robot interaction," The International Journal of Robotics Research, vol. 37, no. 11, pp. 1421–1444, 2018.

[9] Y. Michel, C. Ott, and D. Lee, "Safety-aware hierarchical passivity-based variable compliance control for redundant manipulators," IEEE Transactions on Robotics, vol. 38, no. 6, pp. 3899–3916, 2022.

[10] B. Capelli, C. Secchi, and L. Sabattini, "Passivity and control barrier functions: Optimizing the use of energy," IEEE Robotics and Automation Letters, vol. 7, no. 2, pp. 1356–1363, 2022.

[11] R. J. Adams and B. Hannaford, "Stable haptic interaction with virtual environments," IEEE Transactions on robotics and Automation, vol. 15, no. 3, pp. 465–474, 1999.

[12] K. Samuel, K. Haninger, and S. Oh, "Integrated dob-based approach for admittance control of an industrial robot," in 2023 23rd International Conference on Control, Automation and Systems (ICCAS). IEEE, 2023, pp. 259–264.

[13] D. Ko, D. Lee, W. K. Chung, and K. Kim, "On the performance and passivity of admittance control with feedforward input," in 2022 IEEE/RSJ International Conference on Intelligent Robots and Systems (IROS). IEEE, 2022, pp. 11 209–11 215.

[14] F. Ferraguti, C. Talignani Landi, L. Sabattini, M. Bonfe, C. Fantuzzi, and C. Secchi, "A variable admittance control strategy for stable physical human–robot interaction," The International Journal of Robotics Research, vol. 38, no. 6, pp. 747–765, 2019.

[15] C. T. Landi, F. Ferraguti, L. Sabattini, C. Secchi, M. Bonfè, and C. Fantuzzi, "Variable admittance control preventing undesired oscillating behaviors in physical human-robot interaction," in 2017 IEEE/RSJ International Conference on Intelligent Robots and Systems (IROS). IEEE, 2017, pp. 3611–3616.

[16] V. Okunev, T. Nierhoff, and S. Hirche, "Human-preference-based control design: Adaptive robot admittance control for physical human-robot interaction," in 2012 IEEE RO-MAN: The 21st IEEE International Symposium on Robot and Human Interactive Communication. IEEE, 2012, pp. 443–448.

[17] V. Duindam and S. Stramigioli, "Port-based asymptotic curve tracking for mechanical systems," European Journal of Control, vol. 10, no. 5, pp. 411–420, 2004.

[18] F. Ferraguti, C. Secchi, and C. Fantuzzi, "A tank-based approach to impedance control with variable stiffness," in 2013 IEEE international conference on robotics and automation. IEEE, 2013, pp. 4948–4953.

[19] F. Voigt, A. Naceri, and S. Haddadin, "I 2 mpedance-a passivity based integrative impedance controller for precise and compliant manipulation and interaction," in 2023 IEEE/RSJ International Conference on Intelligent Robots and Systems (IROS). IEEE, 2023, pp. 4472–4479.

[20] C. T. Landi, F. Ferraguti, L. Sabattini, C. Secchi, and C. Fantuzzi, "Admittance control parameter adaptation for physical human-robot interaction," in 2017 IEEE international conference on robotics and automation (ICRA). IEEE, 2017, pp. 2911–2916.

[21] F. Califano, D. van Dijk, and W. Roozing, "A task-based post-impact safety protocol based on energy tanks," IEEE Robotics and Automation Letters, vol. 7, no. 4, pp. 8791–8798, 2022.

[22] C. Ott, A. Kugi, and Y. Nakamura, "Resolving the problem of non-integrability of nullspace velocities for compliance control of redundant manipulators by using semi-definite lyapunov functions," in 2008 IEEE international conference on robotics and automation. IEEE, 2008, pp. 1999–2004.

[23] A. Dietrich, X. Wu, K. Bussmann, C. Ott, A. Albu-Schäffer, and S. Stramigioli, "Passive hierarchical impedance control via energy tanks," IEEE Robotics and Automation Letters, vol. 2, no. 2, pp. 522–529, 2016.

[24] Y. Michel, C. Ott, and D. Lee, "Passivity-based variable impedance control for redundant manipulators," IFAC-PapersOnLine, vol. 53, no. 2, pp. 9865–9872, 2020.

[25] A. De Luca, A. Albu-Schaffer, S. Haddadin, and G. Hirzinger, "Collision detection and safe reaction with the dlr-iii lightweight manipulator arm," in 2006 IEEE/RSJ International Conference on Intelligent Robots and Systems. IEEE, 2006, pp. 1623–1630.

[26] H. Khalil, Nonlinear Systems, ser. Pearson Education. Prentice Hall, 2002.